Results on intense beam focusing and neutralization from the neutralized beam experiment[a)]

P. K. Roy, S. S. Yu,[b)] S. Eylon, E. Henestroza, A. Anders, F. M. Bieniosek, W. G. Greenway, B. G. Logan, W. L. Waldron, and D. L. Vanecek
Lawrence Berkeley National Laboratory, 1 Cyclotron Road, Berkeley, California 94720

D. R. Welch and D. V. Rose
Mission Research Corporation, 5001 Indian School Road NE, Albuquerque, New Mexico 87110-3946

R. C. Davidson, P. C. Efthimion, E. P. Gilson, and A. B. Sefkow
Princeton Plasma Physics Laboratory, Princeton, New Jersey 08543-0451

W. M. Sharp
Lawrence Livermore National Laboratory, 7000 East Avenue, L-645, Livermore, California 94550

(Received 31 October 2003; accepted 9 December 2003; published online 23 April 2004)

Experimental techniques to provide active neutralization for space-charge-dominated beams as well as to prevent uncontrolled ion beam neutralization by stray electrons have been demonstrated. Neutralization is provided by a localized plasma injected from a cathode arc source. Unwanted secondary electrons produced at the wall by halo particle impact are suppressed using a radial mesh liner that is positively biased inside a beam drift tube. Measurements of current transmission, beam spot size as a function of axial position, beam energy, and plasma source conditions are presented along with detailed comparisons with theory. © *2004 American Institute of Physics.*
[DOI: 10.1063/1.1652712]

I. INTRODUCTION

Final focusing has been a subject of intense study[1–3] from the very early days of heavy ion fusion (HIF). Neutralized ballistic transport (NBT)[4–11] is presently being studied for propagating intense heavy ion beams inside a reactor chamber to an inertial confinement fusion (ICF) target. A recent HIF driver study[12] demonstrates that stringent final-focus requirements[13–15] can be met, provided that active neutralization is implemented to overcome the formidable space charge of the intense ion beams. Other beam transport schemes under consideration include self-pinched transport[16–20] and discharge channel[21–23] transport.

In the NBT scheme, the individual beams focus outside of the target chamber and enter through ports in the chamber walls. These beams are focused and directed such that they intersect before striking the target and then strike the target as they are expanding into an annular configuration.[24] The target chamber is filled at low pressure with a gas such as flibe. A volumetric plasma is produced as the flibe gas is partially ionized by the beam as well as by x rays emitted by the hot target.

The volumetric plasma is not adequate to provide the necessary neutralization. Therefore, additional plasma, the ''plasma plug,'' is externally injected near the chamber entry port, through which the beam passes. Chamber transport using annular and solid plasma regions in the transport chamber have been examined numerically by several investigators.[17,18,25] The general concept studied in this paper consists of an initially non-neutralized beam passing through a finite thickness of plasma and dragging along plasma electrons for partial charge and current neutralization.

An earlier experiment[26] examined the charge neutralization of a heavy ion beam by electrons drawn from a localized source as the beam was focused. The electron source was a glowing tungsten filament placed in the beam path, enabling the supply of thermionically emitted electrons inside of the beam. The experiment demonstrated the beneficial effect of charge neutralization on a heavy-ion beam, and these results were confirmed in a series of electrostatic particle-in-cell (PIC) simulations.

To quantitatively ascertain the various mechanisms for neutralization, the Neutralized Transport Experiment (NTX) was constructed at Lawrence Berkeley National Laboratory. In this experiment a high quality beam is passed through well-characterized plasma sources. The objective is to provide sufficiently detailed experiment data to validate simulation code predictions. Here, we are presenting initial results of neutralization from localized plasma plug on the NTX. In this article we describe the neutralization physics, NTX beamline system, techniques to control stray electrons in vacuum transport, and beam neutralization using a plasma plug.

II. PHYSICS OF NEUTRALIZATION

The plasma plug provides electrons that neutralize to >90% the charge of a convergent beam. Typically, $n_p/Zn_b > 1$, where n_p is the plasma density and n_b and Z are the ion beam density and charge state. Ideally, the plasma is in electrical contact with a conducting boundary at large radius,

[a)]Paper UI2 2, Bull. Am. Phys. Soc. **48**, 333 (2003).
[b)]Invited speaker.

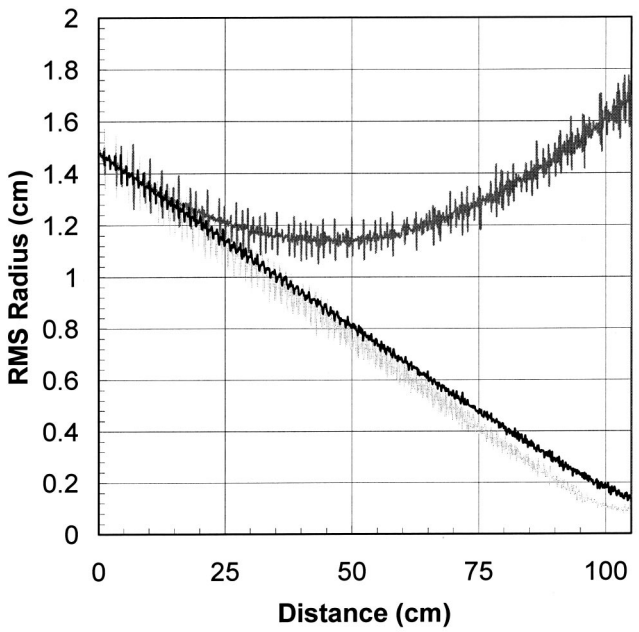

FIG. 1. A comparison of the beam envelope for simulations with perfect neutralization (the lower line), no neutralization or vacuum (the top line), and a MEVVA source or plasma plug (middle line).

enabling a continuous supply of electrons. Stationary plasma can only provide an ion beam electron neutralization down to some minimum space-charge potential. The key scaling parameter for beam transport is the dimensionless perveance defined as the ratio of the beam space charge to kinetic energy ($K=2I_b/I_A\beta_i^2$, where $I_A=\beta_i\gamma_i m_i c^3/eZ$ is the Alfvén current with a beam of current I_b, velocity $\beta_i c$, and relativistic factor γ_i). Provided $Km_i/Zm_e>1$, electrons from this plasma can accelerate in the beam space-charge potential to the beam velocity. This condition limits the minimum residual space charge potential to $1/2m_e v_i^2$.[27] Previous neutralization experiments[26,28] have provided, to some degree, confirmation of this limit.

Plasma neutralization in NTX was simulated with the PIC code LSP.[13,14] The low emittance ($\epsilon\sim 30\pi$ mm mrad) of the NTX beam at the entrance to the neutralized region allows for the beam to be focused to a small spot (1–2 mm radius). Several $r-z$ LSP simulations were run using the NTX geometry with a nominal 255 keV, 24 mA singly charged potassium ion beam, assuming the beam envelope is circular. The beam enters the neutralization pipe ($z=0$) with a 2 cm outer radius and a 20 mrad convergence angle. Figure 1 shows the beam envelope radius for three simulations with perfect neutralization (ballistic), no neutralization (vacuum), and a MEVVA source-generated plasma (plasma plug) described in the next section with a maximum $10^{10}\,\mathrm{cm}^{-3}$ density. With no neutralization, the simulation gives a 1.64 cm radius at this distance. With the perfect neutralization, we calculate yields a 1 mm rms spot at focus ($z=100$ cm). Including the MEVVA plasma yields a spot only slightly larger than ballistic (1.35 mm at $z=100$ cm). In this case, the plasma electrons provide a source of comoving electrons with a 96% effective neutralization.

III. DESCRIPTION OF NTX BEAMLINE

NTX consists of three major sections: a potassium source chamber,[29] a magnetic transport section with four pulsed quadrupoles,[30] and a 1 m long neutralization drift section with a plasma plug.[31] Figure 2 shows a sketch of the NTX beamline. A thorough description of the design and characterization of this NTX beamline has been submitted recently for publication.[32] We now describe the major sections of NTX.

A. Ion source

The K^+ beam is produced on a standard hot-plate source,[33] with the perveance being determined by passing the beam through a metal aperture after the diode. Pulsed power is provided by a Marx generator that was used in the Multiple Beam Test Experiment (MBE-4).[34] A timed crowbar switch on NTX produces pulses with 0.5–1 μs rise time and a 10 μs "flat top."

B. Magnetic beam transport

The section consists of four pulsed quadrupole magnets separated by short drift regions. The quadrupole fields are

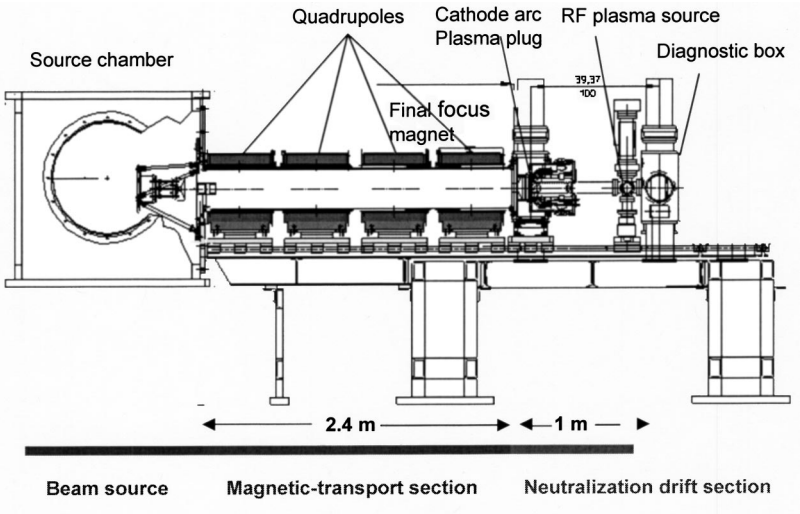

FIG. 2. A schematic of the NTX beamline setup.

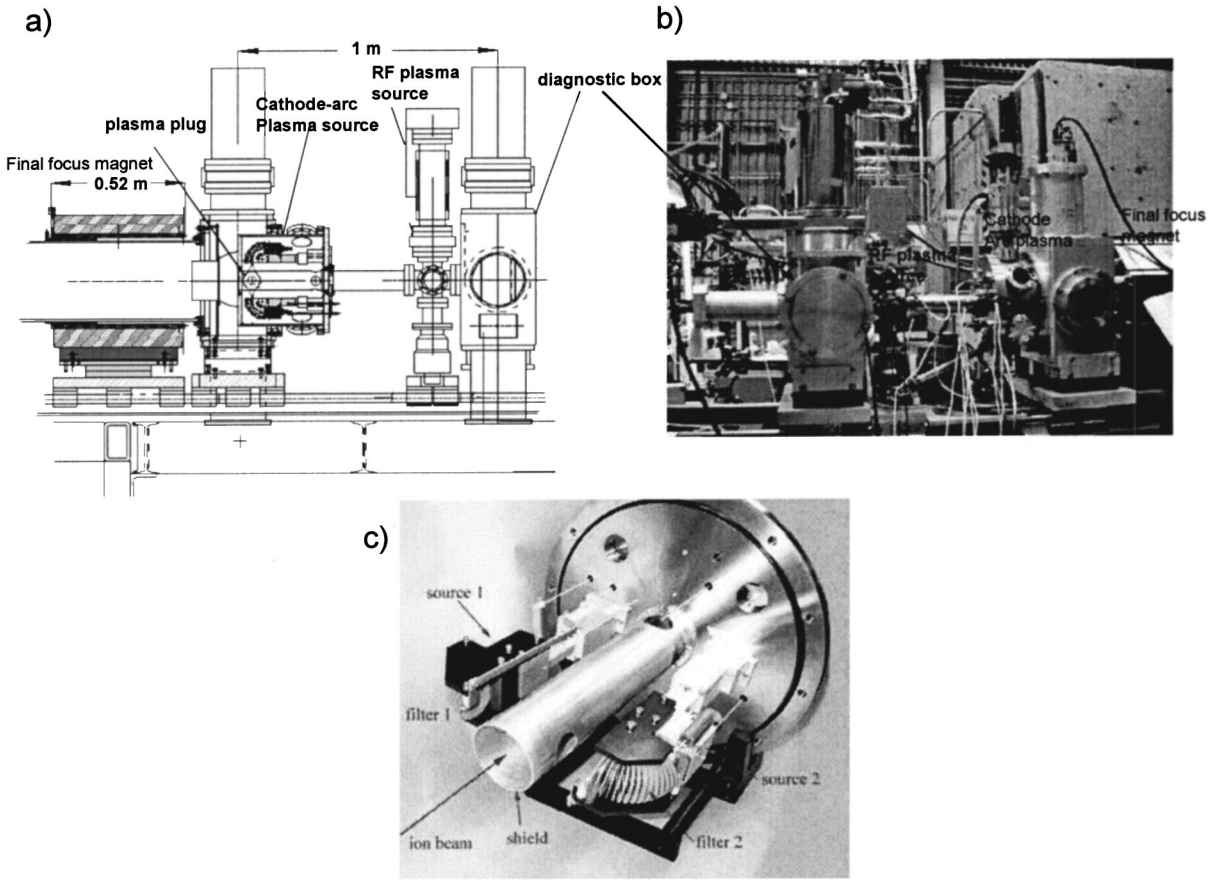

FIG. 3. (a) A schematic of the 1 m long neutralization section with the location of the plasma sources, (b) the neutralization section on NTX, and (c) the cathode arc plasma source.

chosen to obtain a beam with 1 m focal length (20 mm radius and 20 mrad convergence angle) at the entrance to the neutralization region. The choice of a 60 cm half-lattice period and 2.4 m total length is a scaled version of a driver design.

C. Plasma source and focusing section

Figure 3 shows (a) the schematic of a 1 m long neutralization section indicated the location of the different plasma sources, (b) the neutralization section on NTX, and (c) the cathode arc plasma source. We now present results using the cathode arc plasma source referred to as the MEVVA plasma plug throughout the article. The plasma density of the MEVVA plasma plug can be estimated by noting that the ion current is given generally by $j_i = zen_i\nu_i$, where j_i is the ion current density, z is the average charge state number (1.7), e is the elementary charge, n_i is the ion number density, and ν_i is the average ion velocity (1.54×10^5 m/s) in the direction of the collector, which is here identical with the plasma flow velocity. With an area of collection of about $10^{-2}\,\mathrm{m}^2$, one obtains $n_i \approx 1.8\times10^{10}\,\mathrm{cm}^{-3}$ for the average plasma density inside the metal shield at about 250 μs after arc triggering, at a pulse-forming network (PFN) charging voltage of 2.0 keV. We find that the NTX cathode-arc source produces plasmas with densities in the 10^{10}–$10^{11}\,\mathrm{cm}^{-3}$ ranges and that the plasma density is proportional to the discharge voltage up to 2.5 keV.

D. Optical imaging technique for beam profile

The non-neutralized and neutralized beam were recorded using modern optics. We have used glass and ceramic (98% alumina) as scintillator materials. Charge neutralization was provided by a high-transparency (80%–90% transmission) metallic mesh placed on or near the surface of the scintillator. By applying a negative bias to the mesh, stray external electrons were decelerated and deflected away from the scintillator, limiting their contribution to the optical image to negligible levels. Time-resolved beam-induced images on the scintillator screen were captured with a Roper Scientific gated intensified CCD camera viewing the scintillator through a vacuum window, and images are processed using the public-domain program ImageJ.

IV. BEAM TRANSPORTATION IN VACUUM

A. Uncontrolled neutralization

As a preliminary step to characterize beam transport in the NTX final-focus system, a 255 keV beam was injected

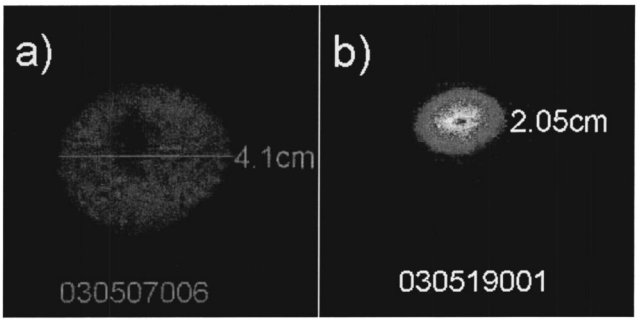

FIG. 4. Beam images for a 255 keV beam measured 1 m downstream, transported through a tube of diameter (a) 15 cm and (b) 7.6 cm.

into a 15 cm diameter pipe from the exit of the final focus magnet to 1 m downstream, ensuring that electron emission from the walls was negligible. Later, in order to use the beam with a matching system of the MEVVA plasma plug and the final focus drifting section, it was transported through a nominal 7.6 cm diameter beam. Figure 4 shows beam images for a beam transported through the (a) 15 cm and (b) 7.6 cm diameter tube. A smaller spot size, roughly 50% less in diameter, was measured for transport in the 7.6 cm diameter tube, which did not agree well with the calculated beam transport in a vacuum. This smaller size was due to the capture by the beam of free electrons from the wall that partially neutralized the beam.

B. Control technique of uncontrolled neutralization

Ions from the poorly matched beam front and halo ions in the main pulse of the beam can strike the outer wall of the transport tube. A single ion impact can produce thousands of secondary electrons depending on the energy and angle of incidence[35,36] with ions of grazing-angle incidence producing the largest secondary electron yield.[37] Only a small fraction of the beam ions striking the wall are needed to provide a space-charge-limited supply of electrons from the wall. If the secondary electrons are not stopped, they are attracted to the beam potential and can provide some degree of beam neutralization. Halo scrape-off will be drastically reduced using the 15 cm pipe. Also, for a larger wall radius, the wall electrons can spend only a small fraction of their time within the beam. The electrons are moving at their greatest velocity while passing through the beam, further decreasing their beam neutralization. Thus, the neutralization fraction from these electrons will scale no better than the ratio of the beam to wall radii. A wall radius comparable to that of the beam will provide some sizable degree of neutralization and prevent the observation of expected ''vacuum transport.'' The secondary electrons are produced with mean energy roughly that of the ionization potential of the impacted wall atoms—typically 10 eV. The distribution of electrons in ionization events also has a high-energy tail falling off as the square of the energy. Thus, if we place a highly transparent wire mesh sleeve within the drift tube and bias it with potential $\geqslant$10 eV, we can expect to collect these secondary electrons and prevent them from moving into the beam path. Given a positive potential, electrons produced on the mesh itself will tend to

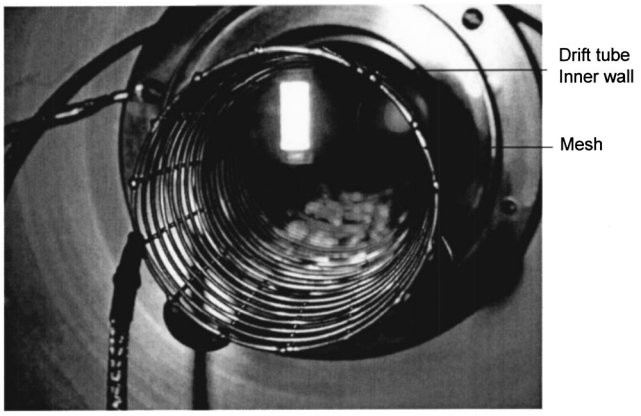

FIG. 5. Cylindrical metal mesh of outer diameter 6.3 cm was installed inside a 7.6 cm diameter beam drift tube.

be trapped near the mesh. Figure 5 shows a high beam transference cylindrical tube shape metal mesh that was inserted into the 7.6 cm beam tube. The thickness and longitudinal length of the mesh were 2.2 mm, and 58.2 cm, respectively. Outer and inner diameters of the mesh tube were 6.3 and 5.88 cm, respectively, thus maintaining better than a 5 mm radial electrical isolation from the beam tube wall. Figure 6 shows a pattern of beam profiles corresponding to energies for vacuum transport in (a) WARP calculation, the (b) 15 cm diameter tube and (c) 7.6 cm diameter tube using the mesh bias of positive 1 keV. Using the mesh bias, the measured beam profile was in general agreement with WARP for vacuum transport. Figure 7 shows the measured beam profile for varying mesh bias. In Fig. 7(a), the lower line with solid circles shows that a beam diameter of 2.4 cm was measured with 0 V across the mesh bias for 255 keV beam energy. A beam diameter of roughly 3.75 cm was also measured by applying $\pm$500 V across the mesh for the same beam energy, shown by lines of solid diamonds and cross symbols, respectively. The line with hollow circles shows a measured beam diameter of 3.75 cm using a mesh bias of $+$250 V. A larger beam diameter of 4 cm was measured with a mesh bias of $\pm$1 keV for the same 255 keV beam energy, as shown by

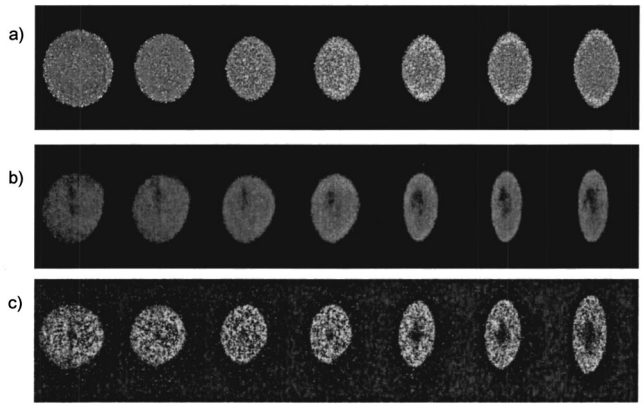

FIG. 6. Beam profile for vacuum transport for 240–310 keV beam energies from (a) WARP calculations, (b) experimental measurements for transport through a 15 cm diameter tube, and (c) experimental measurements for transport through a 7.6 cm diameter tube using mesh bias of $+1$ keV.

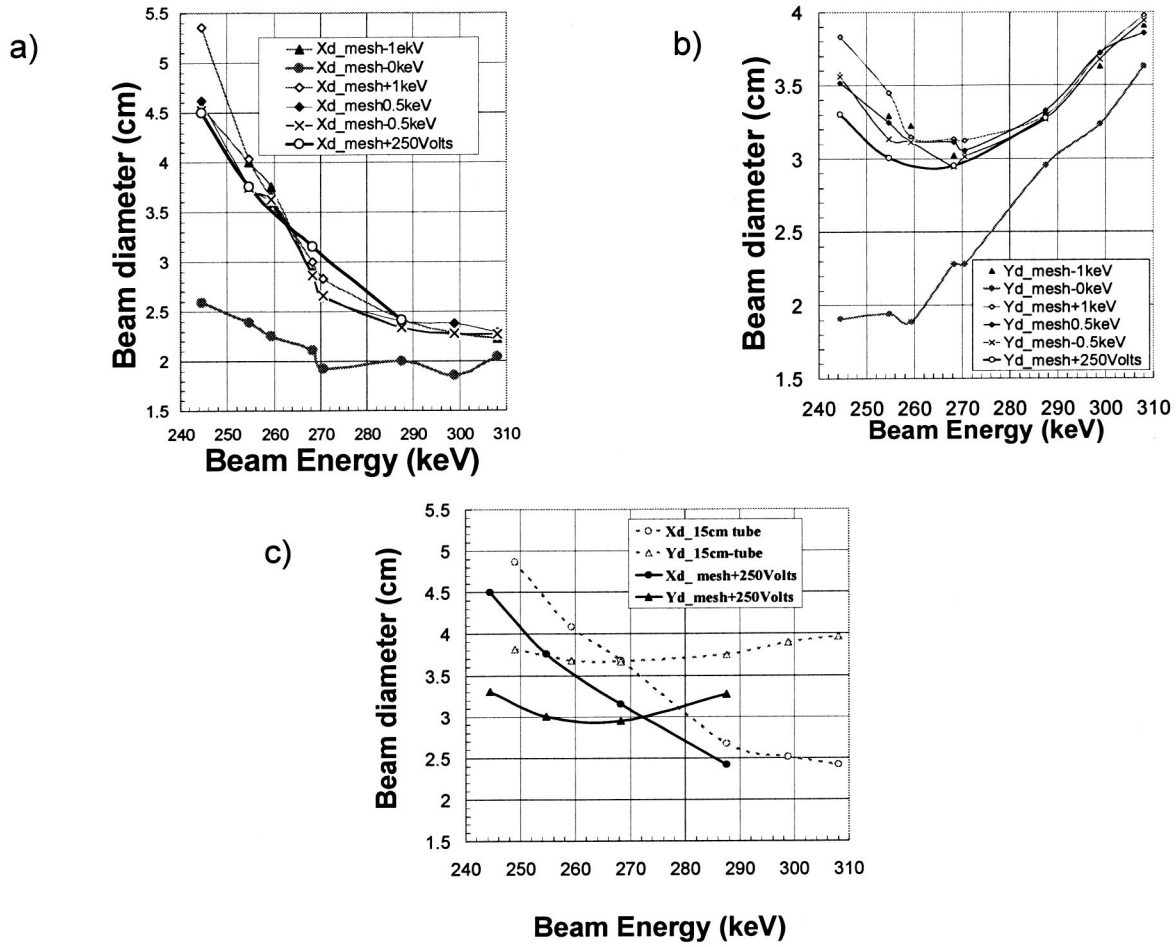

FIG. 7. Beam diameters corresponding to beam energies were measured in the (a) *x* axis and (b) *y* axis by varying mesh bias, and (c) a comparison of beam size for a 255 keV beam transported through a 15 cm tube (dotted lines for the *x*-*y* axis) and the mesh included 7.6 cm diameter tube (solid lines for the *x*-*y* axis) with bias 250 V.

lines of hollow diamond and solid triangle symbols in the figure. The positive 250 V bias on the mesh provides a smooth trend of beam shape, regardless of beam energies in the range of 245 to 300 keV.

Beam diameter measurement by varying beam energies was performed in a 15 cm diameter vacuum tube separately, where the possibility of a wall–electron effect was negligible. There was no mesh or plasma inside the tube that could influence measurements of ion beam transport in vacuum conditions. Figure 7(c) shows a comparison of beam diameters for transportation through the mesh embedded 7.6 cm diameter tube with a bias of +250 V and 15 cm diameter vacuum tube. The dotted lines with hollow circles and triangles represent beam diameters that were measured in the *x* and *y* axis, respectively, for a beam of energies 240–310 keV transported through the 15 cm diameter tube. Diameters of 4.53, 4.0, and 2.68 cm were measured in the *x* axis for the beam of energies 259, 268, and 298 keV, respectively. On the other hand, the lines with solid circles and triangles represent beam diameters that were measured in the *x* and *y* axis, respectively, for a beam of energies 244 to 290 keV transported through the 7.6 cm diameter tube. Beam diameters of 3.76, 3.15, and 2.41 cm were measured in the *x* axis for the beam of 255, 268, and 287 keV, respectively. These were end-to-end measurements of a beam image, without the deduction of any cutoff value that was used for statistical error reduction in Sec. V. For a 255 keV beam, a difference of 6 mm in beam diameter was measured between the two cases. This difference was smaller for a more energetic beam. For example, for a 288 keV beam, a difference of 2 mm in diameter was measured for the two cases. For a higher-energy beam (say 300 keV), the radial distance of the beam from the wall was larger than the lower-energy beam (255 keV), and neutralization was not significant. By using the mesh and an appropriate voltage across it, we were still achieving a slightly smaller size than ''expected'' for an un-neutralized beam. The difference in the two cases, as we inferred, was due to the 58.2 cm mesh liner in the 7.6 cm diameter tube was not long enough to cover the entire 1 m long drift tube. As a result, partial neutralization occurred beyond the ends of the mesh. However, the mesh was a significant development in overcoming uncontrolled neutralization of wall electrons.

Currents corresponding to positive and negative voltages across the mesh were measured during a 255 keV beam pulse. Figure 8 shows experimental data of current measure-

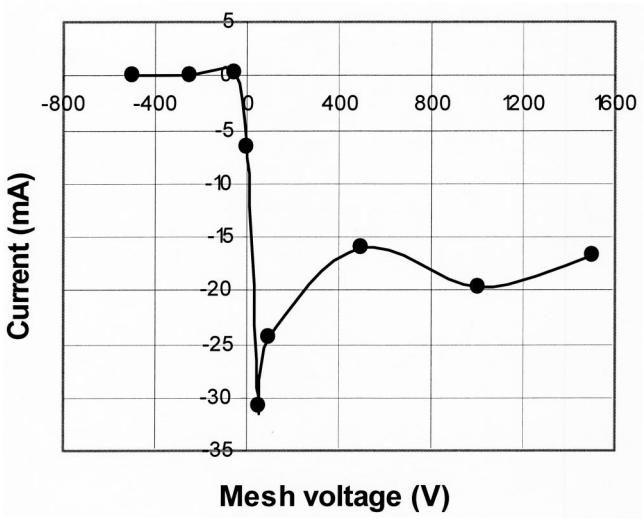

FIG. 8. Current in mesh varying mesh bias during a 255 keV beam pulse.

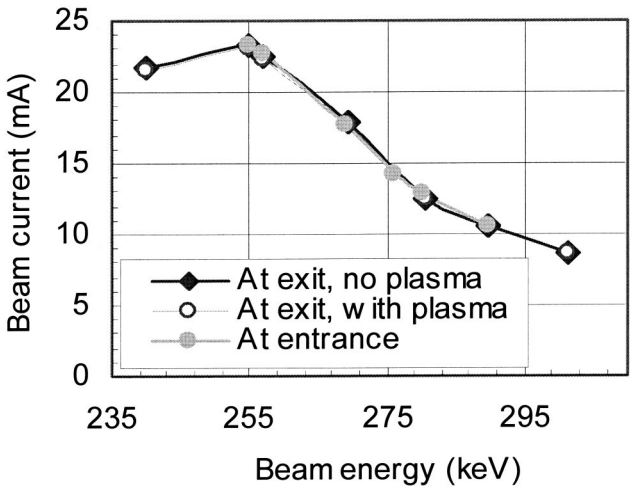

FIG. 9. Measured beam current. The solid circles are the symbols of currents, measured at the entry of the 1 m final focus section or on the other way at the exit of the magnets. The solid diamonds in the line are the symbols of currents, measured at the end of the 1 m drift section and the symbol hollow circles represent MEVVA plasma plug neutralized beam current.

ments in the mesh. A negative current of 6.56 mA was measured at a zero potential across the mesh, which shows that secondary or wall electrons movement exist and only that electrons which were directly striking the mesh wire were measured and inferred that uncollected electrons remaining around the mesh. A positive 50 V potential was applied across the mesh to collect these all electrons; a current of negative 30.72 mA was measured. Voltages such as negative 250 V and negative 500 V were also applied to the mesh; however, no significant current was measured. It was inferred that a higher negative potential, like negative 250 V, across the mesh was able to completely stop radial inward and outward motion of electrons, but leaving uncollected electrons. Therefore, collection of all the electrons around the mesh, using a +250 V potential, was a better choice. However, the presence of a higher mesh bias has some effect of the physics of plasma neutralization. For a positive potential, plasma electrons initially accelerated up to the beam velocity as they leave the plasma, are then accelerated up to an energy corresponding to the mesh bias. The quiescent comoving plasma electrons now have a velocity many times that of the beam. As the mesh potential increases, these electrons become more inefficient at neutralizing the beam potential and a larger beam focal spot is expected. For a negative potential, the plasma plug electrons are largely excluded from the beam in the region of the mesh yielding no neutralization.

V. BEAM NEUTRALIZATION

A. Beam current

Beam current was measured at the exit of final focus [at the diagnostic box in Fig. 3(a)] with and without plasma, and at the entrance of final focus (at the end of final focus magnet). In order to measure beam current, a Faraday cup was used. The cup was biased with a +500 V and its internal guard ring was biased with a negative 900 V. An electron trap was installed in front of the Faraday cup. Figure 9 shows beam currents as a function of energies for beam aperture at the entrance of the neutralization drift section. All measurements overlap each other and show 100% beam current transport in the system. There was no significant beam loss in the drift section, and full beam current was transported before neutralization and during neutralization.

B. Neutralized beam

The ion beam was neutralized using plasma electrons from the MEVVA plasma (described in Sec. III C). A series of neutralized beam spot size measurements is underway with various conditions and parameters. Figure 10 shows a viewgraph of beam images for a (a) non-neutralized and (b) a neutralized beam of energy 255 keV. In both cases the beam was transported through a 7.6 cm diameter tube (the mesh bias was +250 V). The rms beam radius (using higher and lower cutoff values) of the non-neutralized beam was 14.7 mm (end-to-end eye view rms radius was 16.4 mm), and the rms radius of the neutralized beam was 1.26 mm.

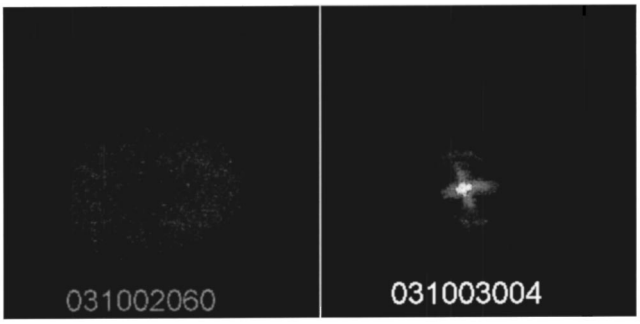

FIG. 10. Beam images for a non-neutralized (left) and neutralized (right) beam of energy 255 keV. In both cases beam was transported through a 7.6 cm diameter tube (the mesh bias was +250 V).

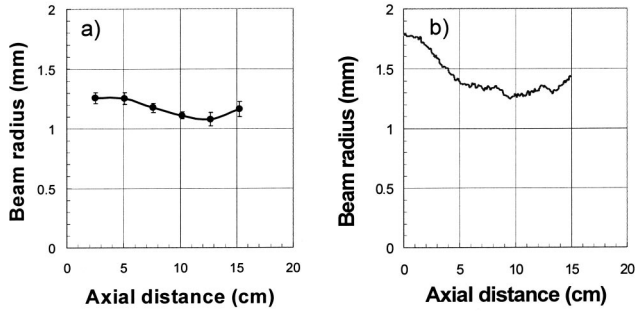

FIG. 11. Axial beam envelope variations in the (a) 7.6 cm drift tube (the mesh bias with +250 V) and (b) theoretical calculation (without mesh).

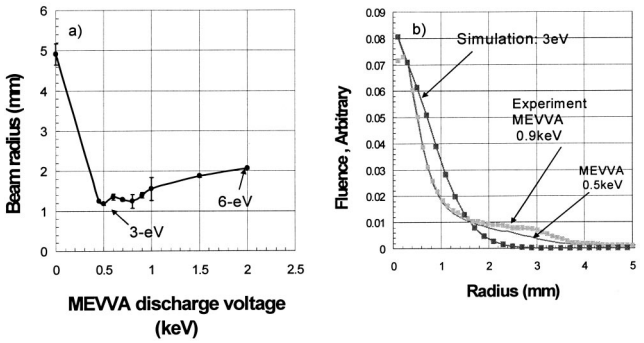

FIG. 13. (a) Neutralized beam radius versus plasma discharge voltage; (b) a comparison between experiment and theory of the radial distribution profile.

These measurements show that a vacuum transport beam was compressed approximately 90% of its volume by beam neutralization.

The variation of the neutralized beam radius with axial position was measured at the diagnostic box by varying the scintillator position over a range of around 15 cm. Figure 11 shows axial beam envelope variations in (a) an experiment using mesh with +250 V inside the 7.6 cm drift tube and (b) a theoretical calculation without mesh consideration. Though the discrepancy in beam radius is less than a millimeter, this difference might be due to the absence of mesh in the calculation. However, we are very close to understanding the neutralized beam envelope for the final focus.

The radius of the neutralized NTX beam was also measured for various beam energies (produced using the Marx crowbar pulse system) and for various time delays in image recording. Figure 12 shows (a) the variation of a neutralized beam radius corresponding to beam energies, (b) the beam pattern from head-to-tail by varying the time delay of image recording, and (c) the variation of multiple Marx wave forms for a same condition. For the energy variation, sensitivity to chromatic variation is a result of magnetic quadrupole optics.

To ascertain the head to tail variation of the pulse, a 255 keV beam was transported through a meshless 7.6 cm diameter tube through plasma produced with 2 keV discharge potential. Time slices of 100 ns width were recorded with 253 gain and delays between 4.6 and 12.8 μs in intervals of 0.2 μs. It was observed that the beam head and tail have halos. We inferred that the longitudinal forces due to the beam space charge were increasing the velocity of the beam head and slowing the beam tail. Although the beam radius looks flat for a time delay of 6–11 μs, a closer examination shows that the beam radius variation was of order 0.2 mm. This might be due to shot to shot variation of Marx voltage, as shown in wave the forms in Fig. 12(c), or the variation of charges accumulation in the capacitor tank of the MEVVA plasma plug high-voltage system.

The neutralized beam radius was also a function of the MEVVA plasma discharge voltage. Figure 13 shows (a) the beam radius versus the plasma discharge voltage, and (b) a comparison between experiment and theory of the radial distribution profile. The basic size of the beam spot is similar in both cases (experiments and theory) with differences attrib-

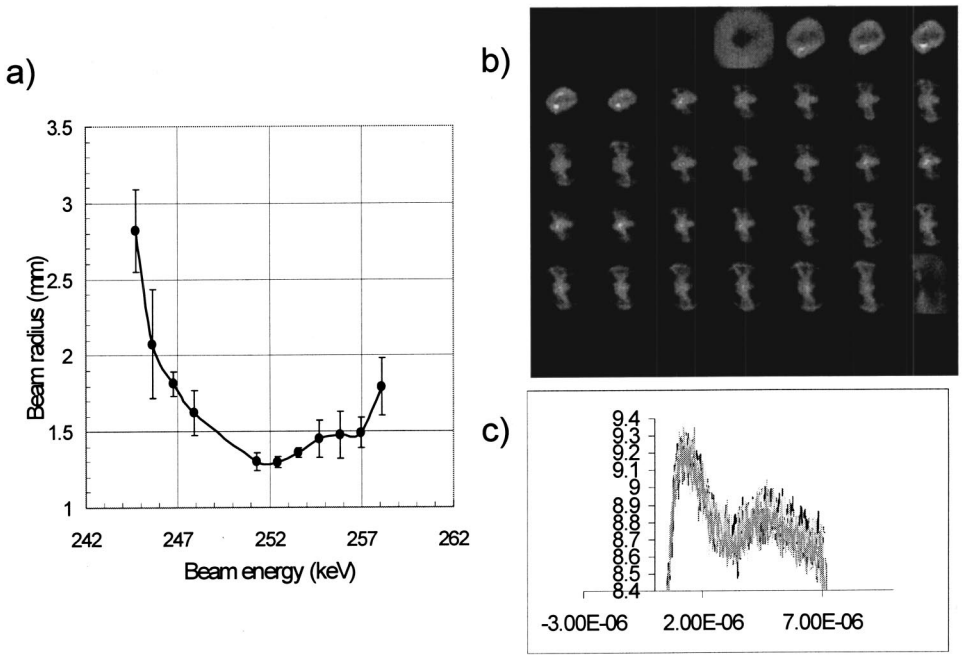

FIG. 12. Shows (a) variation of the neutralized beam radius corresponding to beam energies, (b) beam pattern from head to tail by varying the time delay of image recording, (c) the shot-to-shot variation of Marx wave forms.

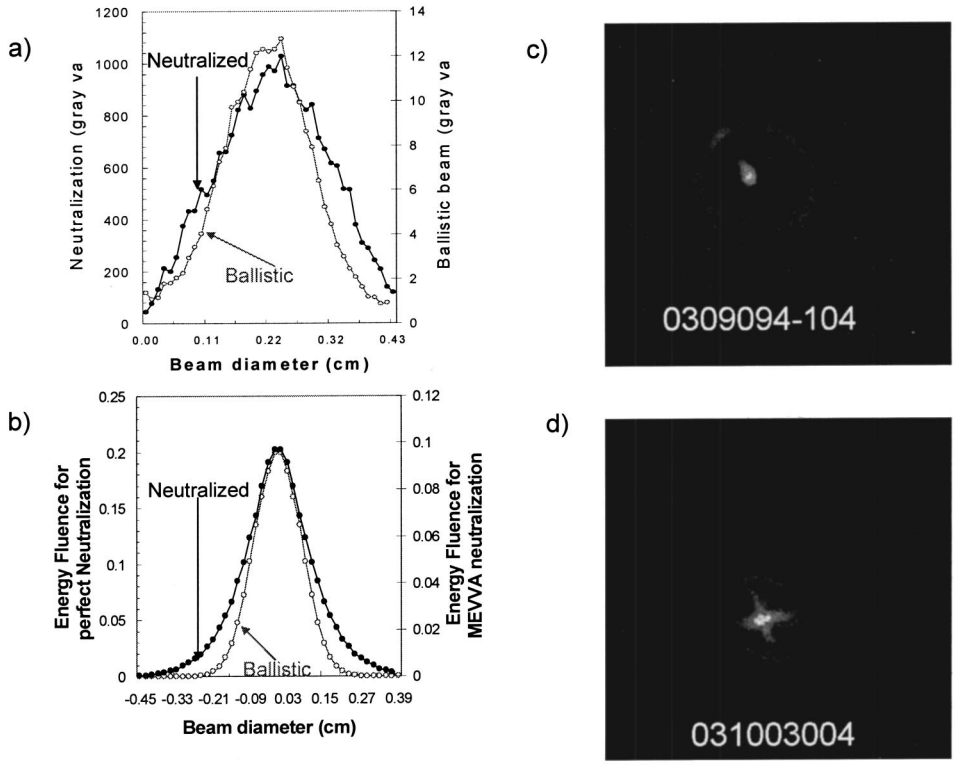

FIG. 14. A comparison of (a) the line integral profile of experimental ballistic beam and plasma neutralized beam; (b) the LSP theoretical simulation for the beams; (c) experimental ballistic beam image; and (d) the MEVVA neutralized beam image.

uted to a halo due to nonlinear focusing seen in the experimental curve. Simulations show that if an electrical connection is maintained to the pipe wall through electron space-charge-limited emission (SCLE), the beam spot shows little variation for plasma densities ranging from $3\times10^{8}-3\times10^{10}\,\mathrm{cm}^{-3}$ for an initial plasma temperature of 3 eV. For a 6 eV initial plasma temperature, which is greater than $1/2m_e v_i^2$, the beam spot size was roughly 50% larger than the case with 3 eV plasma [Fig. 13(a)]. The sensitivity of the beam spot to incoming beam emittance is calculated to be weak with only a 30% spot-size variation for a factor of 3 change in emittance. This low sensitivity to emittance indicates that charge neutralization in the NTX experiment should be quite close to that 96% value seen in simulations and not influenced by details in the emittance.

C. Neutralized and ballistic beams

The neutralized NTX beam radius was compared with that of an array of pinhole beamlets. Since the pinhole beam has a negligible space charge and emittance, its trajectory is effectively ballistic. Each beamlet was formed by passing the beam through a system of two cross slits. The aggregate beamlet radius is then compared with radius of the unattenuated beam neutralized with the MEVVA plasma source. Figure 14 shows comparison of (a) the line integral profile of an experimental ballistic beam and plasma neutralized beam, (b) LSP theoretical simulation for the beams, (c) the experimental ballistic beam image, and (d) the MEVVA neutralized beam image. Here, we see good agreement between theory and experiments. As expected, we observe the profile of the neutralized beam is slightly larger than the pinhole beam image due to the effect of the residual space charge.

VI. CONCLUSION

Several experiments have recently been carried out on the Neutralized Transport Experiment (NTX) at Lawrence Berkeley National Laboratory. We have demonstrated experimentally that a biased cylindrical mesh inside a drift tube can prevent uncontrolled neutralization of a space-charge-dominated ion beam. Without neutralization, the NTX beam radius at the nominal 1 m focal distance is found to be 14.7 mm with the mesh, compared with about 10 mm without, in better agreement with the 16.4 mm value found in numerical simulations. When the NTX beam is neutralized by passing it through a MEVVA plasma, the focal radius decreases to 1.26–1.4 mm, compared with the 1 mm spot size found in simulations for perfect neutralization. Another recent experiment has shown that the variation of the non-neutralized NTX beam radius with an axial position near the focal point qualitatively matches theoretical predictions. Finally, good agreement is found between the radial fluence profile of a neutralized NTX beam and an effectively ballistic beam made by passing the full NTX beam through a pinhole.

ACKNOWLEDGMENTS

The authors are grateful to all scientific members and technical staff of the Heavy Ion Fusion Virtual National Laboratory (HIF-VNL).

This work was performed under the auspices of the U.S. Department of Energy by University of California Lawrence Livermore National Laboratory and Lawrence Berkeley National Laboratory under Contracts No. W-7405-ENG-48 and No. DE-AC-3-76SF00098.

[1]W. B. Herrmannsfeldt (private communications); *ERDA Summer Study of Heavy Ions for Inertial Fusion*, edited by R. O. Bangerter, W. B. Herrmannsfeldt, D. L. Judd, and L. Smith, LBL-5543, California, 1976, p. 25.
[2]See National Technical Information Service Document Conf. No. 780979 (S. S. Yu, H. L. Buchanan, E. P. Lee, and F. W. Chambers, in *Proceedings of the Heavy Ion Fusion Workshop*, edited by R. C. Arnold, ANL-79-41, 1978, p. 403). Copies may be ordered from the National Technical Information Service, Springfield, VA 22161.
[3]See National Technical Information Service Document Conf. No. 791012 (C. L. Olson, in *Proceedings of the Heavy Ion Fusion Workshop*, Berkeley, California, 1979, edited by W. B. Herrmannsfeldt, LBL-10301, SLAC-PUB-2575, UC-28, 1980, p. 403). Copies may be ordered from the National Technical Information Service, Springfield, VA 22161.
[4]N. Barboza, Fusion Eng. Des. **32–33**, 453 (1996).
[5]D. A. Callahan, Fusion Eng. Des. **32–33**, 44 (1996).
[6]B. G. Logan and D. A. Callahan, Nucl. Instrum. Methods Phys. Res. A **415**, 468 (1998).
[7]J. L. Vay and C. Deutsch, AIP Conf. Proc. **406**, 267 (1997).
[8]W. M. Sharp, D. A. Callahan-Miller, R. B. Langdon, and M. S. Armel, Bull. Am. Phys. Soc. **44**, 201 (1999).
[9]I. D. Kaganovich, G. Shvets, E. Startsev, and R. C. Davidson, Phys. Plasmas **8**, 4180 (2001).
[10]D. V. Rose, D. R. Welch, B. V. Oliver, R. E. Clark, W. M. Sharp, and A. Friedman, Nucl. Instrum. Methods Phys. Res. A **464**, 299 (2001).
[11]D. R. Welch, D. V. Rose, B. V. Oliver, and R. E. Clark, Nucl. Instrum. Methods Phys. Res. A **464**, 134 (2001).
[12]S. S. Yu, W. R. Meier, R. P. Abbott *et al.*, Fusion Sci. Technol. **44**, 266 (2003).
[13]T. P. Hughes, R. E. Clark, and S. S. Yu, Phys. Rev. ST Accel. Beams **2**, 110401 (1999).
[14]D. R. Welch, D. V. Rose, B. V. Oliver, and R. E. Clark, Nucl. Instrum. Methods Phys. Res. A **464**, 134 (2001).
[15]W. Sharp, D. A. Callahan, D. P. Grote, M. Tabak, E. Henestroza, S. S. Yu, D. V. Rose, D. R. Welch, and P. F. Peterson, in *Proceedings of the 2003 Particle Accelerator Conference*, edited by J. Chew, P. Lucas, and S. Webber (IEEE, Piscataway, NJ, 2003), p. 2637.
[16]K. Hahn and E. Lee, Fusion Eng. Des. **32–33**, 417 (1996).
[17]C. L. Olson *et al.*, Proceedings of the 16th International Atomic Energy Agency Fusion Energy Conference, 1996, p. 195.
[18]D. R. Welch and C. L. Olson, Fusion Eng. Des. **32–33**, 477 (1996).
[19]D. V. Rose, P. F. Ottinger, D. R. Welch, B. V. Oliver, and C. L. Olson, Phys. Plasmas **6**, 4094 (1999).
[20]P. F. Ottinger, F. C. Young, S. J. Stephanakis, D. V. Rose, J. M. Neri, B. V. Weber, M. C. Myers, D. D. Hinshelwood, D. Mosher, C. L. Olson, and D. R. Welch, Phys. Plasmas **7**, 346 (2000).
[21]A. Tauschwitz, S. S. Yu, S. Eylon, R. O. Bangerter, W. Leemans, C. Peters, J. O. Rasmussen, L. Reginato, J. J. Barnard, and W. M. Sharp, Fusion Eng. Des. **32–33**, 493 (1996).
[22]R. R. Peterson and C. L. Olson, AIP Conf. Proc. **406**, 259 (1997).
[23]S. Yu, S. Eylon, T. Fessenden *et al.*, Nucl. Instrum. Methods Phys. Res. A **415**, 174 (1998).
[24]D. A. Callahan-Miller and M. Tabak, Nucl. Fusion **39**, 883 (1999).
[25]D. R. Welch, D. V. Rose, B. V. Oliver, T. C. Genoni, R. E. Clark, C. L. Olson, and S. S. Yu, Phys. Plasmas **9**, 2344 (2002).
[26]S. A. MacLaren, A. Faltens, P. A. Seidl, and D. V. Rose, Phys. Plasmas **9**, 1712 (2002).
[27]C. L. Olson, AIP Conf. Proc. **152**, 215 (1986).
[28]C. L. Olson, D. L. Hanson, J. W. Poukey, and D. R. Welch, Fusion Eng. Des. **32–33**, 485 (1996).
[29]S. Eylon, E. Henestroza, P. Roy, and S. S. Yu, in Ref. 15, p. 2626.
[30]D. B. Shuman, S. Eylon, E. Henestroza, P. K. Roy, W. Waldron, S. S. Yu, and T. Houck, in Ref. 15, p. 2628.
[31]S. S. Yu, A. Anders, F. M. Bieniosek *et al.*, in Ref. 15, p. 98.
[32]E. Henestroza, S. Eylon, P. K. Roy, S. S. Yu *et al.*, ''Design and characterization of a neutralized-transport experiment for heavy-ion fusion,'' Phys. Rev. ST Accel. Beams (submitted).
[33]D. Baca, J. W. Kwan, and J. K. Wu, in Ref. 15, p. 3294.
[34]W. M. Fawley, T. Garvey, S. Eylon, E. Henestroza, A. Faltens, T. J. Fessenden, K. Hahn, L. Smith, and D. P. Grote, Phys. Plasmas **4**, 880 (1997).
[35]P. H. Stoltz, M. A. Furman, J.-L. Vay, A. W. Molvik, and R. H. Cohen, Phys. Rev. ST Accel. Beams **6**, 054701 (2003).
[36]R. E. Kirby and F. K. King, Nucl. Instrum. Methods Phys. Res. A **469**, 1 (2001).
[37]G. F. Dionne, J. Appl. Phys. **44**, 5361 (1973).